

Resonant triad dynamics in weakly damped Faraday waves with two-frequency forcing

J. Porter^{a,b,*}, M. Silber^a

^a *Department of Engineering Sciences and Applied Mathematics, Northwestern University, Evanston, IL 60208, USA*

^b *Department of Applied Mathematics, University of Leeds, Leeds LS2 9JT, UK*

Received 15 January 2003; received in revised form 20 August 2003; accepted 12 September 2003

Communicated by A. Doelman

Abstract

Many of the interesting patterns seen in recent multi-frequency Faraday experiments can be understood on the basis of three-wave interactions (resonant triads). In this paper we consider two-frequency forcing and focus on a resonant triad occurring near the bicritical point where two pattern-forming modes with distinct wavenumbers onset simultaneously. This triad has been observed directly (in the form of rhomboids) and has also been implicated in the formation of quasipatterns and superlattices. We show how the symmetries of the undamped unforced problem (time translation, time reversal, and Hamiltonian structure) can be used, when the damping is weak, to obtain general scaling laws and additional qualitative properties of the normal form coefficients governing the pattern selection process near onset; such features help to explain why this particular triad is seen only for certain “low” forcing ratios, and predict the existence of drifting solutions and heteroclinic cycles. We confirm the anticipated parameter dependence of the coefficients and investigate its dynamical consequences using coefficients derived numerically from a quasipotential formulation of the Faraday problem due to Zhang and Viñals.

© 2003 Elsevier B.V. All rights reserved.

PACS: 05.45.–a; 47.20.Ky; 47.54.+r; 47.35.+i

Keywords: Resonant triads; Faraday waves; Pattern formation; Symmetry-breaking

1. Introduction

When a container of fluid is shaken vertically with sufficient strength, patterns of standing waves (SW) develop on the free surface. This well-known transition, first described by Faraday [1], is one of the best known examples of a pattern-forming instability. At a critical value of the forcing amplitude the flat surface becomes unstable to small perturbations and gives way to a spatially structured state. This excited state is often highly ordered and may take the form of rolls, squares, hexagons, and more exotic structures such as superlattices and quasipatterns of 8-, 10-, or 12-fold rotational symmetry [2–6]. The temporal spectrum of these SW oscillations is highly ordered as

* Corresponding author. Present address: Department of Applied Mathematics, University of Leeds, Leeds LS2 9JT, UK.

Tel.: +44-113-343-5149; fax: +44-113-343-5090.

E-mail address: jport@maths.leeds.ac.uk (J. Porter).

well. In typical Faraday experiments forced with a single frequency ω the first pattern to appear is a *subharmonic* response [7], i.e., it is $2T$ -periodic in time where $T = 2\pi/\omega$. The associated wavenumber k is determined by the dispersion relation $\Omega(k)$ for gravity–capillary waves through the subharmonic resonance condition $\Omega(k) = \omega/2$. This frequency ω , which controls the spatial length scale, and the forcing amplitude f are the most readily accessible control parameters.

Recently, a number of investigators [4–6,8–12] have considered more general kinds of periodic forcing. These forcing functions with multiple frequency components offer a greater number of adjustable parameters. One advantage of this is that the competition between modes of different length scales can be studied in a controlled manner. If the applied acceleration $f(t)$ is composed of two commensurate frequencies $m\omega$ and $n\omega$ (m and n coprime integers):

$$f(t) = \frac{1}{2}(f_m e^{im\omega t} + f_n e^{in\omega t} + \text{c.c.}) = |f_m| \cos(m\omega t + \phi_m) + |f_n| \cos(n\omega t + \phi_n), \quad (1)$$

an appropriate balance between $|f_m|$ and $|f_n|$ ensures that two modes (one driven primarily by the f_m forcing and the other by f_n) onset simultaneously. This *bicritical* point is the natural organizing center for the two-frequency problem because it is at this point that the greatest variety of patterns evolve and compete with each other while still in the weakly nonlinear regime. A complete description of this competition is exceedingly difficult to achieve, yet a number of simple resonant interactions have emerged as crucial building blocks for many of the more interesting patterns. Resonant triads, as the lowest order nonlinear interaction, are particularly influential because they produce a strong coupling between the phases of the three waves involved. They have been implicated in a number of pattern formation studies, both experimental [3–5,8,13] and theoretical [10,14–17].

In this paper we consider the two-frequency forcing (1) and focus on a simple three-wave interaction, occurring near the bicritical point, in which two wavevectors from one critical circle, \mathbf{k}_1 and \mathbf{k}_2 , generate a third wavevector $\mathbf{k}_3 = \mathbf{k}_1 + \mathbf{k}_2$ on the second critical circle (see Fig. 1). Patterns composed of these three modes were called two-mode rhomboids by Arbell and Fineberg [8]. The same basic resonance, however, is a crucial component of more complicated states such as 8- and 10-fold symmetric quasipatterns (the former observed with three-frequency forcing), and several other multiple-mode and modulated states [3,8]. One of the most striking facts about this resonant triad is that it has so far been seen only with forcing ratios of 1:2 (as part of a superlattice-II type state [3]), 2:3, and 4:5. In [9] we showed that the absence of two-mode rhomboids for larger values of m and n is related to the influence of time translation symmetry. This paper provides additional details behind that result as well as others in [9], and explores their dynamical implications.

Symmetry arguments, in general, play a central role in our understanding of pattern formation. In the context of amplitude equations, symmetry constraints determine which type of nonlinear terms can be present and which cannot [18]. In Faraday systems of large aspect ratio (i.e., where the horizontal extent of the system is large compared to the characteristic wavelength) the relevant spatial symmetry is that of the plane, described by the Euclidean group $E(2)$. If the pattern is spatially periodic, as is often the case near onset, many useful results (see, e.g. [18,19]) can be obtained

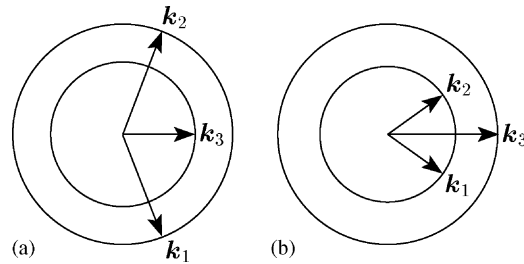


Fig. 1. Resonant triads at the bicritical point. The wavevectors satisfy $\mathbf{k}_3 = \mathbf{k}_1 + \mathbf{k}_2$ and (a) $k_3 = |\mathbf{k}_3| < k_1 = |\mathbf{k}_1| = |\mathbf{k}_2|$, (b) $k_1 < k_3 < 2k_1$.

by restricting to patterns commensurate with this periodic lattice. Temporal symmetries also play an important role in periodically forced systems. In particular, such systems are invariant under discrete translation through one forcing period: $t \rightarrow t + T$. The consequences of this symmetry depend on the nature of the linear eigenfunctions. In the case of single-frequency forcing, for example, the eigenfunctions are subharmonic (i.e., of odd parity under $t \rightarrow t + T$) and the associated \mathbb{Z}_2 symmetry bars all even terms from the evolution equations—the absence of quadratic terms, in particular, means that there are no resonant triad interactions. With two-frequency forcing the constraints of discrete time translation are less severe because the period T is longer than the corresponding period for, say, isolated $m\omega$ forcing, which would be T/m . In this way, modes driven “subharmonically” by f_m can be harmonic with respect to the full period T ; they are harmonic when m is even and subharmonic when m is odd, similarly for n .

In this paper we follow the approach outlined in [9] and extend the usual analysis based on spatial symmetries and discrete time translation to include the (weakly broken) symmetries of continuous time translation, time reversal, and Hamiltonian structure. In [9] we considered hexagons and two-mode superlattices [3,5] as well as two-mode rhomboids, and showed how these symmetries can be used to determine the leading order dependence of important *coefficients* in the SW amplitude equations. In this paper we consider the case of two-mode rhomboids (here simply referred to as resonant triads) in more detail and investigate the dynamical consequences of these (weakly broken) symmetries. In Section 4, for example, we show that a preference for resonant coefficients of opposite sign, which stems from the Hamiltonian structure of the undamped problem, leads to the existence of drifting solutions, modulated waves, and heteroclinic cycles.

The organization of the paper is as follows. In Section 2 we use symmetry to determine the form of the SW amplitude equations and the manner in which the coefficients of these equations depend on the forcing parameters ($m, n, |f_m|, |f_n|, \phi_m, \phi_n$) and on the damping. In Section 3 we test these symmetry-based predictions against coefficients calculated numerically from a quasipotential formulation of the Faraday problem due to Zhang and Viñals [14,15]. Section 4 summarizes the typical dynamics of the resonant triad equations and illustrates with numerical examples the effects of the symmetries discussed in Section 2. Section 5 contains our conclusions.

2. Derivation of the amplitude equations

We use general symmetry arguments to derive the form of the equations governing resonant triads in the presence of two-frequency forcing (1). In particular, we obtain general scaling properties of the normal form coefficients in the limit of weak damping (and forcing). In this limit the problem is constrained not only by spatial symmetries but by the (weakly broken) symmetries of time translation $t \rightarrow t + s, s \in \mathbb{R}$ and time reversal $t \rightarrow -t$ that are features of the unforced inviscid hydrodynamical problem. When these two symmetries are extended as *parameter symmetries* (see also [9]) they apply to the damped forced problem as well. Constraints resulting from full Hamiltonian structure in the undamped forced problem are examined in Section 2.3.

There are many adjustable parameters in the two-frequency Faraday experiment. In addition to the layer depth (assumed to be infinite in the numerical study of Section 3) and fluid properties such as viscosity ν , density ρ , and surface tension Γ , one can vary the basic frequency ω of the driving, the ratio $m:n$ of the two frequency components, their respective magnitudes $|f_m|$ and $|f_n|$, and their phases ϕ_m and ϕ_n . Here we take $1/\omega$ as the unit of time, writing $\tau = \omega t$, and use the wavenumber k_0 associated with $\Omega_0 \equiv \min(m, n)\omega/2$ via the (infinite depth) inviscid dispersion relation $g_0 k_0 + \Gamma k_0^3/\rho = \Omega_0^2$ (g_0 is the acceleration of gravity) as the inverse unit of length. This scaling gives rise to three nondimensional parameters: $\gamma \equiv 2\nu k_0^2/\omega$ (the damping), $\Gamma_0 \equiv \Gamma k_0^3/(\rho\omega^2)$ (the capillarity number), and $G_0 \equiv g_0 k_0/\omega^2$ (the gravity number). The last two are related by $\Gamma_0 + G_0 = (\Omega_0/\omega)^2$.

The situation of interest here is the bicritical point where two modes of distinct wavenumber onset simultaneously as the overall forcing amplitude $f \equiv (|f_m|^2 + |f_n|^2)^{1/2}$ is increased (see Fig. 2). This bistability criteria can be

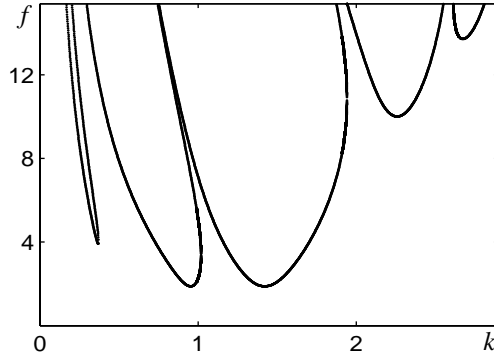


Fig. 2. Neutral stability curves at the bicritical point, calculated using the Zhang–Viñals equations (see Section 3) with $m:n = 3:2$, $\gamma = 0.1$, $\Gamma_0 = 0.5$, $G_0 = 0.5$, $\phi_m = \phi_n = 0$, and $|f_2|/|f_3| \simeq 0.423$. The applied acceleration f is in units of g_0 .

thought of as determining the ratio $|f_m|/|f_n|$. The two critical circles at the bicritical point and the two ways of constructing resonant triads are illustrated in Fig. 1. In either case we take three wavevectors satisfying $\mathbf{k}_3 = \mathbf{k}_1 + \mathbf{k}_2$, $|\mathbf{k}_1| = |\mathbf{k}_2| = k_1$. Without loss of generality we associate \mathbf{k}_1 and \mathbf{k}_2 with the f_m forcing component and \mathbf{k}_3 with the f_n component. Thus Fig. 1a applies if $m > n$ while Fig. 1b applies if $m < n$. When the damping is small each of the excited modes can, to a first approximation, be thought of as a subharmonic response to the corresponding component (f_m or f_n) of the driving. The $e^{ik_1 \cdot x}$ and $e^{ik_2 \cdot x}$ modes oscillate with dominant frequency $m/2$ while the $e^{ik_3 \cdot x}$ mode has dominant frequency $n/2$. Since resonant triads occur only when n is even [11], implying that m is odd since m and n are coprime, we hereafter assume this to be the case.

In the presence of damping the first modes to appear with increasing f are SW. Before turning to the dynamics of SW, however, we consider the form of the equations describing six corresponding traveling wave (TW) modes. In the limit of small damping and forcing a TW expansion is justified even though pure TW solutions are destroyed by the parametric forcing term—such an approach may also be viewed as the unfolding of a Hopf bifurcation (occurring at $\gamma = 0$) with nearly resonant temporal forcing (see [20,21]). Here we are further motivated by the action of the temporal symmetries; TW transform in a simple way under time translation $\tau \rightarrow \tau + s$ and time reversal $\tau \rightarrow -\tau$ whereas SW do not. The simple transformation properties of TW allow us to take full advantage of both the spatial and temporal symmetries of the problem. A center manifold reduction is then used to obtain the equations describing SW near onset.

2.1. Traveling wave equations

We consider a system of six TW with wavevectors \mathbf{k}_1 , \mathbf{k}_2 , and $\mathbf{k}_3 = \mathbf{k}_1 + \mathbf{k}_2$. The surface height $h(\mathbf{x}, \tau)$ is expanded as

$$h(\mathbf{x}, \tau) = \sum_{\pm} Z_1^{\pm} e^{i(\mathbf{k}_1 \cdot \mathbf{x} \pm m\tau/2)} + Z_2^{\pm} e^{i(\mathbf{k}_2 \cdot \mathbf{x} \pm m\tau/2)} + Z_3^{\pm} e^{i(\mathbf{k}_3 \cdot \mathbf{x} \pm n\tau/2)} + \text{c.c.} + \dots \quad (2)$$

Equations describing the slow evolution of the TW amplitudes Z_j^{\pm} , $j = 1, 2, 3$ must be equivariant under the operations of spatial translation (T_{ϕ}), reflection (κ) about a line through \mathbf{k}_3 , and rotation (\mathcal{R}) by π (i.e., inversion through the origin):

$$T_{\phi} : Z_j^{\pm} \rightarrow Z_j^{\pm} e^{i\phi_j}, \quad \phi = (\phi_1, \phi_2), \quad \phi_1, \phi_2 \in [0, 2\pi), \quad \phi_3 = \phi_1 + \phi_2, \quad (3a)$$

$$\kappa : Z_1^{\pm} \leftrightarrow Z_2^{\pm}, \quad (3b)$$

$$\mathcal{R} : Z_j^\pm \rightarrow \bar{Z}_j^\mp. \quad (3c)$$

In addition, they must satisfy the temporal symmetries

$$T_s : (Z_1^\pm, Z_2^\pm) \rightarrow (Z_1^\pm, Z_2^\pm) e^{\pm i m s/2}, \quad Z_3^\pm \rightarrow Z_3^\pm e^{\pm i n s/2}, \quad (f_m, f_n) \rightarrow (f_m e^{i m s}, f_n e^{i n s}), \quad (4a)$$

$$\sigma : Z_j^\pm \rightarrow Z_j^\mp, \quad (\tau, \gamma) \rightarrow -(\tau, \gamma), \quad (f_m, f_n) \rightarrow (\bar{f}_m, \bar{f}_n), \quad (4b)$$

corresponding to time translation (T_s) and time reversal (σ). Since these operations transform parameters as well as dynamical variables, they belong to a more general class of symmetries (for a definition of parameter symmetries see [22]). Time translation and time reversal, when understood in the usual sense (as acting only on phase space), are broken by the presence of forcing and damping, but survive in the sense of Eqs. (4). Although parameter symmetries are often unphysical (it makes little sense to take $\gamma < 0$) they are perfectly good mathematical symmetries of the governing equations and may be used to advantage—in this case they yield the proper form of “symmetry-breaking” terms.

Symmetries (3) and (4) lead to equivariant TW equations of the form

$$\begin{aligned} \dot{Z}_1^+ = & \nu Z_1^+ - (\tilde{\lambda} f_m + \varpi \bar{f}_m^{n-1} f_n^m) Z_1^- + \tilde{\alpha} \bar{f}_m^{(n-2)/2} f_n^{(m-1)/2} \bar{Z}_2^+ Z_3^+ + \delta Z_2^+ \bar{Z}_2^- Z_1^- \\ & + (a|Z_1^+|^2 + b|Z_1^-|^2 + c|Z_2^+|^2 + d|Z_2^-|^2 + e|Z_3^+|^2 + f|Z_3^-|^2) Z_1^+ \\ & + (q_1|Z_1^+|^2 + q_2|Z_1^-|^2 + q_3|Z_2^+|^2 + q_4|Z_2^-|^2 + q_5|Z_3^+|^2 + q_6|Z_3^-|^2) f_m Z_1^- \\ & + (r_1 f_m \bar{Z}_2^+ Z_2^- + \bar{f}_m (r_2 Z_1^+ \bar{Z}_1^- + r_3 Z_2^+ \bar{Z}_2^-) + r_4 f_n \bar{Z}_3^+ Z_3^- + r_5 \bar{f}_n Z_3^+ \bar{Z}_3^-) Z_1^+, \end{aligned} \quad (5a)$$

$$\begin{aligned} \dot{Z}_3^+ = & \varrho Z_3^+ - (\tilde{\mu} f_n + \zeta \bar{f}_m^{n-1} f_n^m) Z_3^- + \tilde{\beta} \bar{f}_m^{(n-2)/2} \bar{f}_n^{(m-1)/2} Z_1^+ Z_2^+ \\ & + (g(|Z_1^+|^2 + |Z_2^+|^2) + h(|Z_1^-|^2 + |Z_2^-|^2) + l|Z_3^+|^2 + p|Z_3^-|^2) Z_3^+ \\ & + (s_1(|Z_1^+|^2 + |Z_2^+|^2) + s_2(|Z_1^-|^2 + |Z_2^-|^2) + s_3|Z_3^+|^2 + s_4|Z_3^-|^2) f_n Z_3^- \\ & + (u_1 f_m (\bar{Z}_1^+ Z_1^- + \bar{Z}_2^+ Z_2^-) + u_2 \bar{f}_m (Z_1^+ \bar{Z}_1^- + Z_2^+ \bar{Z}_2^-) + u_3 \bar{f}_n Z_3^+ \bar{Z}_3^-) Z_3^+, \end{aligned} \quad (5b)$$

where the overdot indicates a derivative with respect to τ . The remaining four equations can be obtained by applying κ and \mathcal{R} . At second and third order in the amplitudes Z_j^\pm we have kept all terms which contribute at leading order (in $\epsilon \sim \gamma \sim |f_m| \sim |f_n|$) to the corresponding SW coefficients (Eqs. (8) of Section 2.2). At the linear level, however, we have included two additional terms (with coefficients ϖ and ζ) that do not contribute at leading order but are responsible for an important qualitative effect, namely, a dependence in the linear problem on the relative phase of the two forcing components—this dependence will be discussed in more detail below. Terms of the form fZ^3 , for example, $q_1|Z_1^+|^2 f_m Z_1^-$ in Eq. (5a), were also found by Zhang [23].

The coefficients in Eqs. (5) are assumed to depend analytically on γ , f_m , and f_n , and must do so in a manner consistent with the temporal symmetries (4). For example, σ (more precisely, $\sigma \circ \mathcal{R}$) forces most coefficients to be purely imaginary at leading order. The real parts, which must be odd under $\gamma \rightarrow -\gamma$, take the form γ , γ^3 , $\gamma|f_m|^2$, etc. Higher order corrections to the imaginary parts, which are even under $\gamma \rightarrow -\gamma$, take the form γ^2 , $\gamma^2|f_m|^2$, and so on; such terms only matter for the detunings $\text{Im}(\nu)$ and $\text{Im}(\varrho)$, where they contribute at leading order to the SW coefficients, and in the parametric forcing coefficients $\tilde{\lambda}$ and $\tilde{\mu}$ where they contribute to a (phase-independent) coupling in the linear SW problem between the two forcing components f_m and f_n —some of the $\mathcal{O}(\epsilon^3)$ terms in the real parts of ν and ϱ contribute to this coupling as well. For these four linear coefficients we therefore write

$$\nu = \gamma(-\nu_r + \hat{\nu}_\gamma \gamma^2 + \hat{\nu}_m |f_m|^2 + \hat{\nu}_n |f_n|^2) + i(\nu_\gamma \gamma^2 + \nu_m |f_m|^2 + \nu_n |f_n|^2), \quad \nu_r > 0, \quad (6a)$$

$$\varrho = \gamma(-\varrho_r + \hat{\varrho}_\gamma \gamma^2 + \hat{\varrho}_m |f_m|^2 + \hat{\varrho}_n |f_n|^2) + i(\varrho_\gamma \gamma^2 + \varrho_m |f_m|^2 + \varrho_n |f_n|^2), \quad \varrho_r > 0, \quad (6b)$$

$$\tilde{\lambda} = \tilde{\lambda}_r \gamma + i(\tilde{\lambda}_i + \tilde{\lambda}_\gamma \gamma^2 + \tilde{\lambda}_m |f_m|^2 + \tilde{\lambda}_n |f_n|^2), \quad (6c)$$

$$\tilde{\mu} = \tilde{\mu}_r \gamma + i(\tilde{\mu}_i + \tilde{\mu}_\gamma \gamma^2 + \tilde{\mu}_m |f_m|^2 + \tilde{\mu}_n |f_n|^2), \quad (6d)$$

while for the remaining coefficients we substitute expansions of the form

$$\varpi = \varpi_r \gamma + i\varpi_i, \quad \tilde{\alpha} = \tilde{\alpha}_r \gamma + i\tilde{\alpha}_i, \quad \delta = \delta_r \gamma + i\delta_i, \quad \dots, \quad (6e)$$

that are truncated at lowest order in both real and imaginary parts. The absence of $\mathcal{O}(1)$ imaginary parts in ν and ϱ results not from symmetry but from the way k_1 and k_3 are defined. These wavenumbers are taken from the (γ -dependent) dual minima of the SW neutral stability curves at the bicritical point (see Fig. 2). One consequence of this implicit γ dependence in k_1 and k_3 is a detuning between the parametrically excited frequencies $m/2$ and $n/2$ and the “natural” frequencies $\Omega(k_1)$ and $\Omega(k_3)$. In the absence of damping and forcing, however, the wavenumbers k_1 and k_3 do satisfy the resonance conditions $\Omega(k_1) = m/2$ and $\Omega(k_3) = n/2$, and the detunings $\text{Im}(\nu)$ and $\text{Im}(\varrho)$ must vanish.

Expansions (6) are consistent (where they overlap) with the analytical formulas derived by Topaz and Silber [10] in the case of one-dimensional waves. Those results also apply to weakly damped Faraday waves with two-frequency forcing, and are based on the Zhang–Viñals equations. The calculations of Topaz and Silber, however, yield no $\mathcal{O}(\epsilon)$ real part to $\tilde{\lambda}$ (i.e., $\tilde{\lambda}_r = 0$); one would likewise expect $\tilde{\mu}_r = 0$. Setting $\tilde{\lambda}_r = \tilde{\mu}_r = 0$ is of no consequence for us because those terms do not contribute at leading order to the SW coefficients of Eqs. (8).

2.2. Standing wave equations

This section contains the results of a standard reduction procedure (see, e.g. [24]) replacing Eqs. (5), near the bicritical point, with a system of three SW amplitude equations. Small deviations from the bicritical point are captured with the reduced forcing parameters $\Delta_m, \Delta_n \in \mathbb{R}$ according to $f_m = f_m^c(1 + \Delta_m)$, $f_n = f_n^c(1 + \Delta_n)$ (a superscript “c” indicates the bicritical value). We find that the critical modes satisfy $Z_j^\pm = e^{\pm i\vartheta_j/2} A_j$, where $\vartheta_1 = \vartheta_2$ and ϑ_3 are the complex phases of $F_m^c \bar{v}^c$ and $F_n^c \bar{w}^c$, respectively, and that the A_j obey

$$\dot{A}_1 = \lambda A_1 + \alpha \bar{A}_2 A_3 + A_1(a|A_1|^2 + b|A_2|^2 + c|A_3|^2), \quad (7a)$$

$$\dot{A}_2 = \lambda A_2 + \alpha \bar{A}_1 A_3 + A_2(a|A_2|^2 + b|A_1|^2 + c|A_3|^2), \quad (7b)$$

$$\dot{A}_3 = \mu A_3 + \beta A_1 A_2 + A_3(d|A_1|^2 + d|A_2|^2 + e|A_3|^2), \quad (7c)$$

where

$$\begin{aligned} \lambda &= \nu_r \gamma \Delta_m + J_1 \gamma^3 \Delta_n + \varepsilon_\lambda \varpi_i (m \Delta_n + (n-1) \Delta_m) |f_m^c|^{n-1} |f_n^c|^m \cos \phi_f, \\ \mu &= \varrho_r \gamma \Delta_n + J_2 \gamma^3 \Delta_m + \varepsilon_\mu \zeta_i (n \Delta_m + (m-1) \Delta_n) |f_m^c|^n |f_n^c|^{m-1} \cos \phi_f, \\ \alpha &= -\varepsilon_\lambda \tilde{\alpha}_i |f_m^c|^{(n-2)/2} |f_n^c|^{(m-1)/2} \cos \Phi, \quad \beta = \varepsilon_\lambda \tilde{\beta}_i |f_m^c|^{(n-2)/2} |f_n^c|^{(m-1)/2} \cos \Phi, \\ a &= J_3 \gamma, \quad e = J_4 \gamma, \quad b = J_5 \gamma - \frac{\tilde{\alpha}_i \tilde{\beta}_i}{2\varrho_r \gamma} |f_m^c|^{n-2} |f_n^c|^{m-1} \sin^2 \Phi, \\ c &= J_6 \gamma + \frac{\tilde{\alpha}_i^2}{2\nu_r \gamma} |f_m^c|^{n-2} |f_n^c|^{m-1} \sin^2 \Phi, \quad d = J_7 \gamma - \frac{\tilde{\alpha}_i \tilde{\beta}_i}{2\nu_r \gamma} |f_m^c|^{n-2} |f_n^c|^{m-1} \sin^2 \Phi. \end{aligned} \quad (8)$$

Here J_1, \dots, J_7 are $\mathcal{O}(1)$ functions of the TW coefficients (6) and are given in Appendix A, $\varepsilon_\lambda = \text{sign}(\tilde{\lambda}_i)$, $\varepsilon_\mu = \text{sign}(\tilde{\mu}_i)$, and

$$\Phi = \varepsilon_\mu \frac{\pi}{4} - \frac{\phi_f}{2}, \quad \text{where } \phi_f = m\phi_n - n\phi_m. \quad (9)$$

The relative phase ϕ_f , associated with the T_s -invariant term $f_n^m \bar{f}_m^n$, is the physically relevant linear combination of ϕ_m and ϕ_n . The coefficients (8) are real and are valid to leading order in ϵ , although additional interesting contributions, not necessarily at lowest order, have been kept as well. In λ and μ , for example, we have included the leading order nonresonant (i.e., lacking explicit dependence on m , n , and ϕ_f) coupling between the two forcings (the $J_1 \gamma^3 \Delta_n$ term in λ and the $J_2 \gamma^3 \Delta_m$ term in μ) and the lowest order “resonant” contribution (the $\mathcal{O}(\epsilon^{m+n-1})$ terms varying as $\cos \phi_f$). In the nonlinear cross-coupling coefficients b , c , and d there is an $\mathcal{O}(\epsilon^{m+n-4})$ resonant contribution coming from the damped SW modes that have been slaved away; this contribution appears at leading order when $m + n \leq 5$.

We now summarize the most important properties of the SW coefficients (8). This structure relies on the parameter symmetries T_s and σ , both possessed by the full hydrodynamical problem [25], and the restriction to weak damping ($\epsilon \ll 1$):

- (1) For $m + n \geq 5$ coefficients (8) are $\mathcal{O}(\epsilon)$ or higher. A similar result was found analytically by Topaz and Silber [10] and Zhang and Viñals [15,23].
- (2) The unfolding parameters λ and μ are linear combinations of Δ_m and Δ_n , and are therefore rotated slightly (and stretched) with respect to the latter, “more natural” parameters. This rotation is $\mathcal{O}(\epsilon^2)$ unless $m:n = 1:2$ when it is $\mathcal{O}(\epsilon)$ and varies as $\cos \phi_f$. Similar rotation is discussed in more detail in [10], although those results are obtained away from the bicritical point.
- (3) When $m + n \leq 5$ the cubic cross-coupling coefficients b , c , and d depend at leading order on the relative phase ϕ_f . This behavior is similar to the leading order phase dependence found by Zhang and Viñals [15] for cubic cross-coupling coefficients with 1:2 forcing, a result obtained perturbatively and not from symmetry considerations. Furthermore, when $m:n = 1:2$ the coefficients b , c , and d diverge as $\epsilon \rightarrow 0$, indicating a failure of the reduction procedure in this limit. This failure is not surprising given that there are three additional critical modes at $\gamma = 0$ that need to be taken into account. The exceptionally strong coupling to these neglected modes when $m:n = 1:2$ (the resonance terms of Eqs. (5), through which the coupling occurs, are otherwise $\mathcal{O}(\epsilon)$ or smaller) explains the dramatic failure of the reduction in that case. In general, the description based on three SW modes is not expected to hold if γ is “too” small.
- (4) Measurable effects relating to coefficients (8) are 2π -periodic in ϕ_f . This is true even for α and β (which appear to be 4π -periodic in ϕ_f ; see Eq. (9)) because Eqs. (7) are invariant under $(A_j, \alpha, \beta) \rightarrow -(A_j, \alpha, \beta)$. Thus, only the *relative* sign of α and β matters; dynamics with Φ and $\Phi \pm \pi$ are equivalent.
- (5) The resonant coefficients α and β are of order $\epsilon^{(m+n-3)/2}$ and thus depend strongly on the choice of forcing frequencies, their influence diminishing exponentially with $m + n$; this fact helps to explain why this type of resonant triad is not seen for large values of $m + n$ [3,8]. The $\epsilon^{(m+n-3)/2}$ dependence is not universal however. Near particular choices of ϕ_m and ϕ_n where $\cos \Phi = 0$ the terms given in Eqs. (8) vanish and, assuming the next nonvanishing term (not calculated) is a factor of γ smaller, there is a crossover to the more extreme $\epsilon^{(n+m-1)/2}$ dependence. Conversely, one could say that resonance effects are *strongest* when $\Phi = 0, \pi$.

2.3. Consequences of Hamiltonian structure

We now examine the implications of full Hamiltonian structure (as opposed to just σ) in the undamped (i.e., inviscid) problem; see [14,17,26–30]. Specifically, we suppose that Eqs. (5) possess a Hamiltonian \mathcal{H} and that the complex amplitudes Z_j^\pm obey the equations of motion (see, e.g. [31–33])

$$\dot{Z}_j^\pm = \mp i \frac{\partial \mathcal{H}}{\partial \bar{Z}_j^\pm}, \quad j = 1, 2, 3. \quad (10)$$

Requiring that \mathcal{H} be a real scalar function invariant under symmetries (3) and (4), one finds that the equations of motion (10) are equivalent to Eqs. (5) only if

$$\begin{aligned}\tilde{\alpha} = \tilde{\beta}, \quad e = g, \quad h = f, \quad q_1 = 2q_2 = 2r_2, \quad q_3 = q_4 = r_1 = r_3, \\ q_5 = q_6 = u_1 = u_2, \quad r_4 = r_5 = s_1 = s_2, \quad s_3 = 2s_4 = 2u_3,\end{aligned}\quad (11)$$

with all coefficients evaluated at $\gamma = 0$. The most important of relations (11) is $\tilde{\alpha} = \tilde{\beta}$ (i.e., $\tilde{\alpha}_i = \tilde{\beta}_i$) because this implies that the resonant coefficients α and β of Eqs. (8) have *opposite signs* for small γ . Although this situation can change with increasing damping, the fact that there is good reason to expect $\alpha\beta < 0$ has profound dynamical implications for Eqs. (7)—it is a prerequisite for a variety of interesting drifting solutions and heteroclinic cycles (see Section 4). Chossat [34] has recently shown that the special form of advective nonlinearities leads to the same conclusion (resonant coefficients of opposite sign) for a general class of self-adjoint hydrodynamical problems (see also [35]). A strict interpretation of the equation $\tilde{\alpha}_i = \tilde{\beta}_i$ (which would also have α and β of equal *magnitude*; see Eqs. (8)) is inappropriate here because, for one thing, such a statement depends on normalization conventions. Provided α and β do not vanish, the amplitudes A_j may always be rescaled to set $|\alpha| = |\beta| = 1$. More to the point, for Eqs. (5) to display “Hamiltonian structure” need not mean that the Z_j^\pm and \bar{Z}_j^\pm are *themselves* canonically conjugate Hamiltonian variables in the sense of Eqs. (10). Transformations (for example, simple rescalings) that preserve dynamics should be allowed as well. Under this relaxed criteria we expect that the oscillations of b , c , and d with Φ will be the same order in magnitude and that the oscillating parts of b and of d (measured with respect to the nonresonant $\mathcal{O}(\epsilon)$ parts) will be strictly negative while that of c is positive. These oscillations appear at leading order only if $m:n = 1:2$ or $3:2$. In the former case they are $\mathcal{O}(\epsilon^{-1})$ and can overwhelm the Φ -independent $\mathcal{O}(\epsilon)$ part.

2.4. Discussion of the amplitude equations

We have related many properties of the coefficients in Eqs. (7) to the influence of (weakly broken) temporal symmetries and Hamiltonian structure. The spatial symmetries of the problem, however, remain fully intact and must be considered as well. They act on the SW (cf. Eqs. (3)) according to

$$T_\phi : A_j \rightarrow A_j e^{i\phi_j}, \quad \phi = (\phi_1, \phi_2), \quad \phi_1, \phi_2 \in [0, 2\pi), \quad \phi_3 = \phi_1 + \phi_2, \quad (12a)$$

$$\kappa : A_1 \leftrightarrow A_2, \quad (12b)$$

$$\mathcal{R} : A_j \rightarrow \bar{A}_j. \quad (12c)$$

In particular, the action of \mathcal{R} explains why the coefficients in Eqs. (7) are real. Note that this nontrivial action of \mathcal{R} on the SW amplitudes, a necessary consequence of the spatial symmetries of the problem, allows for the possibility of symmetry-breaking bifurcations to traveling (hereafter, drifting) waves. Strictly speaking, the “standing waves” of the previous section are standing only on the fast timescale set by ω (i.e., the eigenfunctions satisfy $|Z_j^+| = |Z_j^-|$). On the slow timescale they may or may not drift, depending on whether or not they belong to the \mathcal{R} -invariant subspace (or a translation of it).

Recall that unless n is even there are no quadratic resonant terms, i.e., $\alpha = \beta = 0$. This result, obtained in [11], follows directly from Eqs. (7) by noting that the problem is invariant under a discrete time translation through one period of the forcing—this is the extent to which time translation is usually considered. Accordingly, Eqs. (7) must be equivariant under the operation $(A_1, A_2) \rightarrow (-1)^m (A_1, A_2)$, $A_3 \rightarrow (-1)^n A_3$. If n is even (and therefore m odd) this discrete temporal symmetry is equivalent to the spatial translation $T_{(\pi, \pi)}$ and imposes no additional restrictions [11]. However, if n is odd the induced symmetry forces $\alpha = \beta = 0$. Because we are interested in resonance effects

we always take n to be even. However, even when the resonant coefficients are nonzero there is no guarantee that resonance effects can be easily observed. As seen in Eqs. (8), this depends strongly on $m + n$ and γ . If α and β are extremely small, their influence will be appreciable only while the system is extremely close to onset. Although in one sense this limit is ideally suited for the weakly nonlinear approach taken here, it could prove difficult to conduct experiments in such a restricted regime where the timescale for pattern formation is very long and extraneous factors like noise are important. For this reason it is useful to characterize the range over which resonant terms contribute relative to the range over which the weakly nonlinear analysis is likely to be valid. One can assume, for example, that a weakly nonlinear approach is “justified” when $|A_j| \lesssim \epsilon_0$, where $\epsilon_0 = 0.1$ (or any other reasonable value). The dynamics, however, will begin to switch from resonant (quadratic nonlinearities) to nonresonant (cubic nonlinearities) when these two effects are the same order: $(\alpha, \beta)|A_j|^2 \sim (a, b, c, d, e)|A_j|^3$. For concreteness, we suppose that this transition occurs when $|A_j| \sim \epsilon_{\text{res}} \equiv \max(|\alpha|, |\beta|)/\max(|a|, |b|, |c|, |d|, |e|)$ and denote the ratio of ϵ_{res} to ϵ_0 by η_{res} :

$$\eta_{\text{res}} = \frac{\max(|\alpha|, |\beta|)}{\epsilon_0 \max(|a|, |b|, |c|, |d|, |e|)}. \quad (13)$$

Resonance effects are expected to be important throughout the weakly nonlinear regime if $\eta_{\text{res}} > 1$, while an earlier crossover to nonresonant behavior is anticipated when $\eta_{\text{res}} < 1$. Note that unless $m:n = 1:2$ (this case is more complicated because b, c , and d diverge as $\epsilon \rightarrow 0$) η_{res} scales as $\epsilon^{(m+n-5)/2}$. Broadly speaking, for small γ (i.e., ϵ) one expects that resonance effects will be easy to observe when $m + n \leq 5$ but will become increasingly more delicate as $m + n$ increases.

It is also of interest here to return to Eqs. (5) and examine the linear problem a bit further, in particular, the effect of the phases ϕ_m and ϕ_n on the bicritical point defined by

$$|\nu| = |F_m|, \quad F_m \equiv \tilde{\lambda} f_m + \varpi \tilde{f}_m^{n-1} f_n^m, \quad (14a)$$

$$|\varrho| = |F_n|, \quad F_n \equiv \tilde{\mu} f_n + \zeta f_m^n \tilde{f}_n^{m-1}. \quad (14b)$$

At leading order this bicritical point is independent of ϕ_m and ϕ_n , i.e., the critical amplitudes $|f_m^c|$ and $|f_n^c|$ are uncoupled and we have simply

$$|f_m^c| = \frac{\nu_r}{|\tilde{\lambda}_i|} \gamma, \quad |f_n^c| = \frac{\varrho_r}{|\tilde{\mu}_i|} \gamma. \quad (15)$$

Expressions (15) are utilized throughout this paper (for example, in evaluating coefficients (6a)–(6d) at the bicritical point to obtain expressions (A.1)–(A.7) of Appendix A) and are sufficient to obtain the leading order terms in the SW normal form coefficients (8). However, the lack of phase dependence in Eqs. (15) is contrary to the experimental observations of Müller [12] and the calculations of Zhang and Viñals [15] for the case $m:n = 1:2$. These authors found that there was a strong dependence of $r \equiv |f_m^c|/(|f_m^c| + |f_n^c|)$ on ϕ_n . To see this dependence Eqs. (14) must be solved to high enough order to capture the influence of the $\varpi \tilde{f}_m^{n-1} f_n^m$ and $\zeta f_m^n \tilde{f}_n^{m-1}$ terms. When this is done for $m:n = 1:2$ we find

$$r = \frac{\nu_r |\tilde{\mu}_i|}{\nu_r |\tilde{\mu}_i| + \varrho_r |\tilde{\lambda}_i|} + \frac{\zeta_i \tilde{\mu}_i \nu_r^3 - \varpi_i \tilde{\lambda}_i \nu_r \varrho_r^2}{|\tilde{\lambda}_i|(\nu_r |\tilde{\mu}_i| + \varrho_r |\tilde{\lambda}_i|)^2} \gamma \cos \phi_f, \quad (16)$$

revealing an $\mathcal{O}(\epsilon)$ harmonic dependence on the relative phase ϕ_f . In general, the ϕ_f -dependent correction to r is $\mathcal{O}(\epsilon^{m+n-2})$ and is much less important (with small damping) when $m + n$ is large. For the next available resonant triad interaction, $m:n = 3:2$, it is already of third order. The diminishing influence of ϕ_f with $m + n$ is consistent with the experiments of Edwards and Fauve [4] where no significant phase dependence was found for $m:n = 5:4$. In the case $m:n = 1:2$ we can compare Eq. (16) with [15], where a different convention for the two-frequency

forcing function is used, by setting $\phi_m = \pi/2$ and $\phi_n = \pi/2 + \phi$ (ϕ is the phase variable used in [15]) to find $\phi_f = \phi - \pi/2$. Thus Eq. (16) predicts an extremum for $r(\phi)$ at $\phi = \pi/2$, in agreement with the results of [12,15] (see Fig. 1 of [15])—to be more precise, a maximum was observed at $\phi = \pi/2$. The presence of a maximum rather than a minimum can only be determined from Eq. (16) by computing numerical values for the coefficients $v_r, \tilde{\mu}_i$, etc.

3. Numerical results using the Zhang–Viñals equations

In this section we test the predictions of Eqs. (8) by numerically calculating the SW coefficients from the Zhang–Viñals model [14,15], a quasipotential formulation of the Faraday problem capturing the small-amplitude dynamics of deep fluid layers in the limit of weak damping. This calculation also provides physically relevant coefficients which we use in Section 4 to illustrate SW dynamics. We emphasize that the procedure described here is a direct reduction of the Zhang–Viñals equations at the bicritical point to SW amplitude equations, and does not rely on the symmetries of Section 2.

In the frame of the vibrated fluid one can write the effective gravitational acceleration as $g(t) = g_0 - g_m \cos(m\omega t + \phi_m) - g_n \cos(n\omega t + \phi_n)$, where $g_0 > 0$ is the usual gravitational acceleration. Note that we are picking a convention by using cosines rather than sines, and by putting an overall minus sign in front of the applied acceleration. Switching to the opposite sign convention is equivalent to taking $\phi_m \rightarrow \phi_m + \pi$, $\phi_n \rightarrow \phi_n + \pi$. Because of Eq. (9), we then have $\phi_f \rightarrow \phi_f + (m - n)\pi$ and $\Phi \rightarrow \Phi - (m - n)\pi/2$. Since most of the normal form coefficients in Eqs. (8) depend on ϕ_f this convention does matter. In α, β, b, c , and d it amounts to a shift by $\pi/2$ in the oscillations versus Φ . This follows from the fact that $m - n$ is odd, together with the invariance of the problem under $\Phi \rightarrow \Phi \pm \pi$ (see Section 2.2); changing the above sign convection is thus equivalent (for α, β, b, c , and d) to taking $\Phi \rightarrow \Phi + \pi/2$. The difference is observable—in fact, many other patterns, e.g., hexagons, depend on a phase analogous to Φ (see [9])—but, to our knowledge, even those experiments [3,4,6,8,12] which investigate dependence on the temporal phase (equivalent to ϕ_f) fail to report the convention used (one may infer the convention used in [12] from the agreement found in [15]). Without this information, such results are ambiguous.

The governing equations describing surface height $h(\mathbf{x}, \tau)$ and surface velocity potential $\varphi(\mathbf{x}, \tau)$ are expressed in nondimensional form as

$$\partial_\tau h = \gamma \nabla^2 h + \hat{\mathcal{D}}\varphi - \nabla \cdot (h \nabla \varphi) + \frac{1}{2} \nabla^2 (h^2 \hat{\mathcal{D}}\varphi) - \hat{\mathcal{D}}(h \hat{\mathcal{D}}\varphi) + \hat{\mathcal{D}}(h \hat{\mathcal{D}}(h \hat{\mathcal{D}}\varphi) + \frac{1}{2} h^2 \nabla^2 \varphi), \quad (17a)$$

$$\begin{aligned} \partial_\tau \varphi = & \gamma \nabla^2 \varphi + \Gamma_0 \nabla^2 h - G(\tau)h + \frac{1}{2} (\hat{\mathcal{D}}\varphi)^2 - \frac{1}{2} (\nabla \varphi)^2 - (\hat{\mathcal{D}}\varphi)(h \nabla^2 \varphi + \hat{\mathcal{D}}(h \hat{\mathcal{D}}\varphi)) \\ & - \frac{1}{2} \Gamma_0 \nabla \cdot ((\nabla h)(\nabla h)^2), \end{aligned} \quad (17b)$$

where $G(\tau) = G_0 - f_m \cos(m\tau + \phi_m) - f_n \cos(n\tau + \phi_n)$, and $(f_m, f_n) = (g_m, g_n)k_0/\omega^2$; γ, G_0 and Γ_0 are as defined in Section 2. The nonlocal operator $\hat{\mathcal{D}}$ (see [14]) multiplies each Fourier component by its wavenumber: $\hat{\mathcal{D}} e^{ik \cdot x} = k e^{ik \cdot x}$.

To extract coefficients from Eqs. (17) we use a three-timing perturbation technique (see [16] or [11] for more details), introducing a bookkeeping parameter ε and writing

$$\begin{aligned} h = & \varepsilon h_1 + \varepsilon^2 h_2 + \dots, \quad \varphi = \varepsilon \varphi_1 + \varepsilon^2 \varphi_2 + \dots, \quad f_m = f_m^c + \varepsilon^2 \tilde{f}_m, \\ f_n = & f_n^c + \varepsilon^2 \tilde{f}_n, \quad \partial_\tau \rightarrow \partial_\tau + \varepsilon \partial_{T_1} + \varepsilon^2 \partial_{T_2} + \dots \end{aligned} \quad (18)$$

After h_1 and φ_1 are expressed in terms of Fourier modes, e.g., $h_1(\mathbf{x}, \tau) = \sum_{\mathbf{k}} p_{\mathbf{k}}(\tau) e^{ik \cdot x}$ and $\varphi_1(\mathbf{x}, \tau) = \sum_{\mathbf{k}} q_{\mathbf{k}}(\tau) e^{ik \cdot x}$, the $\mathcal{O}(\varepsilon)$ problem reduces to a series of uncoupled damped Mathieu equations parameterized by the wavenumber k :

$$\partial_{\tau\tau} p_k + 2\gamma k^2 \partial_\tau p_k + (\gamma^2 k^4 + G_0 k + \Gamma_0 k^3) p_k = k(f_m \cos(m\tau + \phi_m) + f_n \cos(n\tau + \phi_n)) p_k. \quad (19)$$

Note from Eq. (17a) that $q_k = k^{-1}(\partial_\tau + \gamma k^2)p_k$. At the bicritical point $(f_m, f_n) = (f_m^c, f_n^c)$ there are exactly two periodic solutions to Eq. (19), $p_{k_1}(\tau)$ and $p_{k_3}(\tau)$, associated with the dual minima of the neutral stability curves (see Fig. 2).

It is worthwhile to extract the leading order linear TW coefficients in Eqs. (5) directly from Eq. (19). First, by setting $\gamma = 0$ and treating f_m and f_n as small perturbations, Eq. (19) can be solved with a multi-timing scheme that gives, as the first solvability conditions,

$$\dot{Z}_1^\pm = -\frac{ik_1 f_m^c Z_1^\mp}{2m}, \quad \dot{Z}_3^\pm = -\frac{ik_3 f_n^c Z_3^\mp}{2n}. \quad (20)$$

Upon comparing Eqs. (20) with Eqs. (5), (6c) and (6d) we identify

$$\tilde{\lambda}_i = \frac{k_i}{2m}, \quad \tilde{\mu}_i = \frac{k_i}{2n}. \quad (21)$$

A complementary treatment with $f_m = f_n = 0$ and γ in the role of small perturbation establishes, via Eqs. (5), (6a) and (6b), that

$$\nu_r = k_1^2, \quad \varrho_r = k_3^2. \quad (22)$$

Eqs. (21) and (22) agree with the formulas given in [10]. In Eqs. (22) we see that the linear damping is proportional to k^2 , as expected. The significance of Eqs. (21), on the other hand, is in relation to the forcing convention discussed above: we have found $\tilde{\lambda}_i > 0$ and $\tilde{\mu}_i > 0$, i.e., that $\varepsilon_\lambda = \varepsilon_\mu = 1$ in Eqs. (8) and (9). Had the alternative convention $g(t) = g_0 + g_m \cos(m\omega t + \phi_m) + g_n \cos(n\omega t + \phi_n)$ been used, we would have found $\varepsilon_\lambda = \varepsilon_\mu = -1$.

Since we assume n is even and m is odd, p_{k_1} is subharmonic with respect to the forcing period 2π : $p_{k_1}(\tau + 2\pi) = -p_{k_1}(\tau)$, while p_{k_3} is harmonic: $p_{k_3}(\tau + 2\pi) = p_{k_3}(\tau)$. To focus on resonant triads, we expand h_1 and φ_1 in terms of the three spatially resonant critical modes (see Fig. 1):

$$h_1 = p_{k_1}(\tau)[A_1(T_1, T_2)e^{ik_1 \cdot x} + A_2(T_1, T_2)e^{ik_2 \cdot x}] + p_{k_3}(\tau)A_3(T_1, T_2)e^{ik_3 \cdot x} + \text{c.c.}, \quad (23a)$$

$$\varphi_1 = q_{k_1}(\tau)[A_1(T_1, T_2)e^{ik_1 \cdot x} + A_2(T_1, T_2)e^{ik_2 \cdot x}] + q_{k_3}(\tau)A_3(T_1, T_2)e^{ik_3 \cdot x} + \text{c.c.}, \quad (23b)$$

At $\mathcal{O}(\varepsilon^2)$ and $\mathcal{O}(\varepsilon^3)$ one obtains differential equations from the solvability conditions. These can be reconstituted by dropping ε and setting $\partial_t = \partial_{T_1} + \partial_{T_2}$. The subsequent equations are identical in form to Eqs. (7), as they must be from symmetries (12). The explicit expressions for these coefficients are in general quite lengthy and must be computed numerically since they involve Fourier representations of $p_k(\tau)$ and $q_k(\tau)$. For this reason we present only numerical results, concentrating mainly on the case $m:n = 3:2$ for which there are many recent experimental results [3,5].

When $m:n = 3:2$ the coefficients α , β , b , c , and d depend at leading order on Φ . We find, however, that for the Zhang–Viñals equations the Φ -independent parts of b , c , and d are considerably larger than the Φ -dependent parts despite the fact that they formally appear at the same order in ε . The most important effect of Φ is therefore in the $\cos \Phi$ behavior of α and β (see Eqs. (8)) which we confirm in Fig. 3. Observe that $\alpha(\Phi)$ and $\beta(\Phi)$ have the opposite phase, i.e., $\alpha\beta < 0$, as predicted by the arguments of Section 2.3. Maximal values of $|\alpha|$ and $|\beta|$ are realized (for small γ) when $\Phi = 0$. We use such an “optimal” choice of phases (e.g., $\phi_m = -\pi/4$ and $\phi_n = 0$) to test in Fig. 4 the scalings predicted by Eqs. (8). Note that, as expected for $m:n = 3:2$, we find $\eta_{\text{res}} \sim 0.02\text{--}0.3$, and resonance effects are likely to be important over much of the weakly nonlinear regime.

For values of Φ near $\pm\pi/2$, the γ dependence of α and β switches from the exponent $(m+n-3)/2$, characteristic of the terms given in Eqs. (8), to the exponent $(n+m-1)/2$, reflecting the next nonvanishing term. Fig. 5 illustrates this second type of behavior by showing $\eta_{\text{res}}(\omega)$, $|\alpha(\gamma)|$, and $|\beta(\gamma)|$ when $\Phi = \pi/2$. The remaining coefficients in Eqs. (7) are essentially unchanged from Fig. 4. Note that $\eta_{\text{res}} \rightarrow 0$ as $\omega \rightarrow 0$ (i.e., $\gamma \rightarrow 0$), indicating that resonance effects

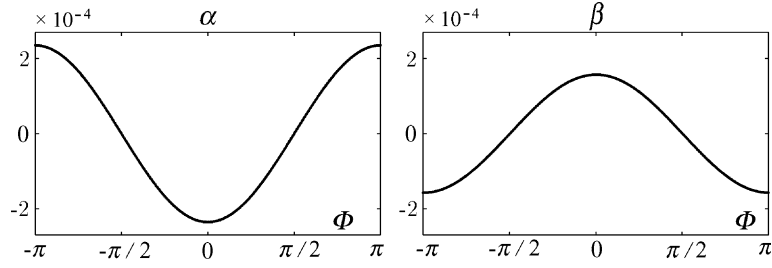


Fig. 3. Dependence of α and β on Φ in the case $m:n = 3:2$ with physical parameters (in cgs units): $\rho = 1$, $\nu = 0.1$, $\Gamma = 21.5$, and $\omega = 10$, corresponding to $\gamma \simeq 2.08 \times 10^{-4}$.

are becoming increasingly weak—larger values of γ are required to see them more easily. Furthermore, besides the fact that α and β are smaller, we find $\alpha\beta > 0$ over the entire calculated range $\omega \in [3, 300]$. This is in sharp contrast to the typical case, with Φ bounded away from $\pm\pi/2$, when the leading order terms given in Eqs. (8) dominate and $\alpha\beta < 0$. Because the relative phase ϕ_f (equivalently, Φ) can alter the sizes of α and β and the sign of their product, it can have a dramatic effect on the dynamics of resonant triads, as shown in the following section.

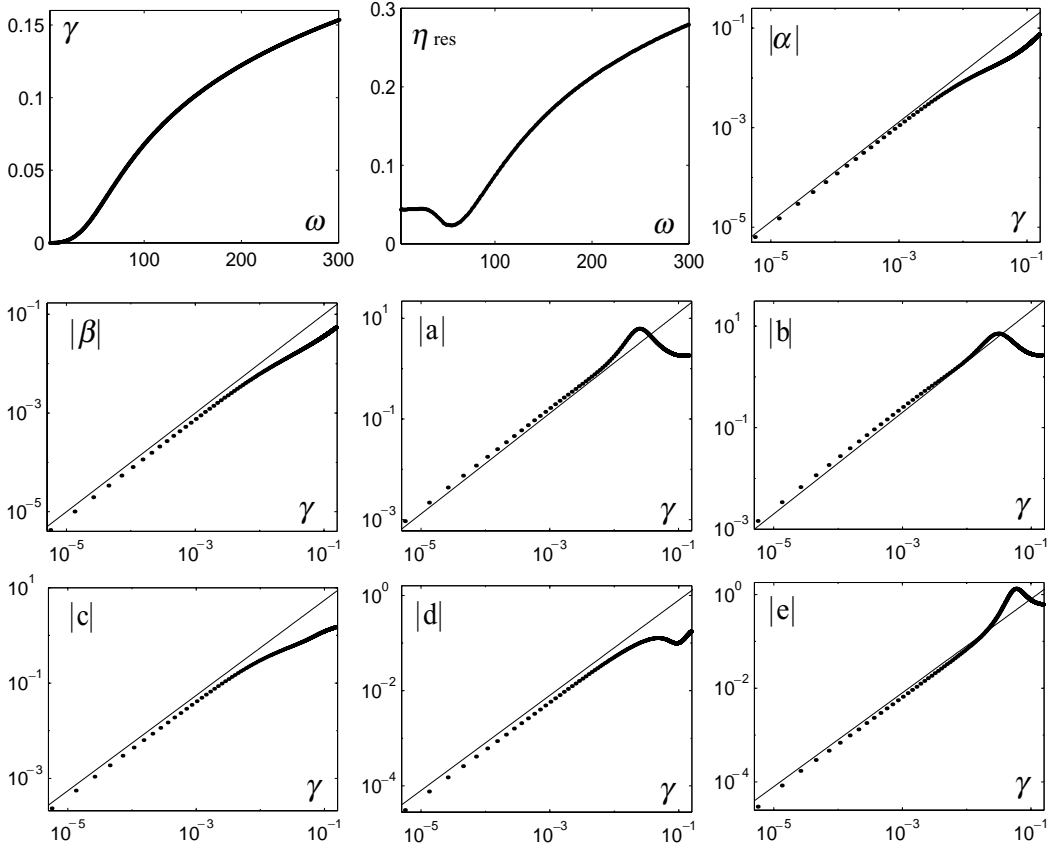


Fig. 4. Behavior of $\gamma(\omega)$, $\eta_{\text{res}}(\omega)$ (see Eq. (13)), and the magnitude of the coefficients $|\alpha(\gamma)|, \dots, |e(\gamma)|$ of Eqs. (7) over the interval $\omega \in [3, 300]$ rad/s with $\Phi = 0$, $\rho = 1$, $\nu = 0.1$, and $\Gamma = 21.5$ (cgs units). The straight lines show the predicted (linear) γ dependence. In the calculation of η_{res} we use $\epsilon_0 = 0.1$.

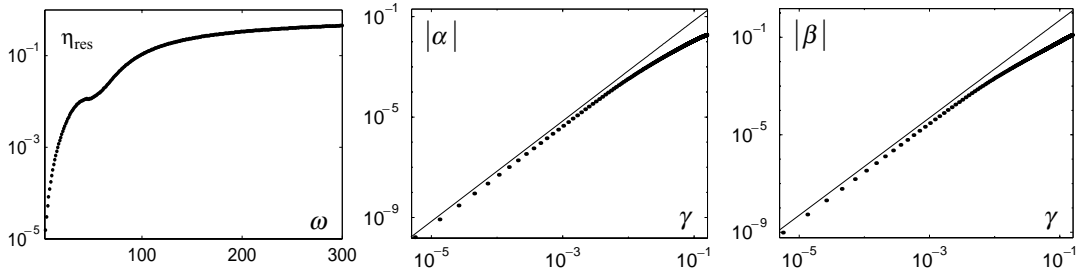


Fig. 5. Dependence of $\eta_{\text{res}}(\omega)$ (using $\epsilon_0 = 0.1$), $|\alpha(\gamma)|$, and $|\beta(\gamma)|$ when $\Phi = \pi/2$. The other parameters are the same as in Fig. 4. Straight lines show the predicted γ^2 dependence.

Table 1
Invariant subspaces of Eqs. (7)

Subspace	Fixed by	Defining property
$\mathcal{U}_{\mathcal{R}}$	\mathcal{R}	$\text{Im}(A_j) = 0$
\mathcal{U}_{κ}	κ	$A_1 = A_2$
\mathcal{U}_1	$T_{(0,\phi)}$	$A_2 = A_3 = 0$
\mathcal{U}_2	$T_{(\phi,0)}$	$A_1 = A_3 = 0$
\mathcal{U}_3	$\kappa, T_{(\phi,-\phi)}$	$A_1 = A_2 = 0$

Table 2
Typical solutions (see text) classified according to the reflection symmetries \mathcal{R} and κ . Dashed lines indicate potential bifurcations

\mathcal{U}_{κ}	$\mathcal{U}_{\kappa} \cap \mathcal{U}_{\mathcal{R}}$	$\mathcal{U}_{\mathcal{R}}$
DW $_{\kappa}$ MDW $_{\kappa}$ HET $_2$	O SR $_3$ MM $_{\kappa}$ MSW $_{\kappa}$ HET $_1$	SR $_1$ MM MSW
<div style="border: 1px solid black; padding: 5px; text-align: center;"> no symmetry DW </div>		

4. Dynamics

In this section we discuss the dynamics of Eqs. (7) with an eye to the influence of relations (8) and (11). As shown by Guckenheimer and Mahalov [36] these dynamics can be very rich, in part because a number of solutions drift or “travel” on the slow time scale, as discussed in Section 2.4. In the following we refer to these as drifting waves (DW) to emphasize that this motion is much slower than the fast (standing) oscillations associated with the parametric forcing.

While the temporal symmetries are now implicit, expressed in relations (8) and (11) describing the scaling, parameter dependence, and relative sign of the SW normal form coefficients, the unbroken spatial symmetries (12) force the existence of dynamically invariant subspaces containing distinct classes of solutions; the most important of these *fixed point subspaces* are listed in Table 1. Not all of these subspaces are isolated and independent. For

example, $\mathcal{U}_{\mathcal{R}}$ contains the solutions that are invariant under inversion through the origin (i.e., under \mathcal{R}) but there is a torus of equivalent subspaces generated by T_{ϕ} ; each of these related subspaces is invariant under inversion through an appropriate (translated) origin. Similarly, there is a circle of subspaces equivalent to \mathcal{U}_{κ} generated by $T_{(\phi, -\phi)}$; solutions in these subspaces satisfy $A_2 = e^{i2\phi} A_1$ and are reflection-symmetric about a line parallel to \mathbf{k}_3 . The subspaces \mathcal{U}_1 and \mathcal{U}_2 are related by the reflection κ and are equivalent. In the following we use $\mathcal{U}_{\mathcal{R}}$, \mathcal{U}_{κ} , and \mathcal{U}_1 to denote the entire family of equivalent subspaces, the representative members of which are listed in Table 1. In practice, the most important subspaces are $\mathcal{U}_{\mathcal{R}}$ and \mathcal{U}_{κ} because they relate to easily recognizable characteristics: solutions in $\mathcal{U}_{\mathcal{R}}$ are strictly standing (i.e., they do not drift; see below) while solutions in \mathcal{U}_{κ} possess a line of symmetry and may drift only in a direction parallel (or antiparallel) to \mathbf{k}_3 .

For most purposes it helps to factor out the continuous translation symmetry T_{ϕ} by writing $A_j = a_j e^{i\theta_j}$ and introducing the T_{ϕ} -invariant phase $\theta = \theta_3 - \theta_1 - \theta_2$. One then obtains the four-dimensional system

$$\dot{r}_1 = \lambda r_1 + \alpha r_2 r_3 \cos \theta + r_1 (a r_1^2 + b r_2^2 + c r_3^2), \quad (24a)$$

$$\dot{r}_2 = \lambda r_2 + \alpha r_1 r_3 \cos \theta + r_2 (b r_1^2 + a r_2^2 + c r_3^2), \quad (24b)$$

$$\dot{r}_3 = \mu r_3 + \beta r_1 r_2 \cos \theta + r_3 (d r_1^2 + d r_2^2 + e r_3^2), \quad (24c)$$

$$\dot{\theta} = - \left(\beta \frac{r_1 r_2}{r_3} + \alpha \frac{r_2 r_3}{r_1} + \alpha \frac{r_1 r_3}{r_2} \right) \sin \theta, \quad (24d)$$

where the θ_j satisfy

$$\dot{\theta}_1 = \alpha \frac{r_2 r_3}{r_1} \sin \theta, \quad \dot{\theta}_2 = \alpha \frac{r_1 r_3}{r_2} \sin \theta, \quad \dot{\theta}_3 = -\beta \frac{r_1 r_2}{r_3} \sin \theta. \quad (25)$$

Eqs. (25) guarantee that solutions in $\mathcal{U}_{\mathcal{R}}$, which corresponds to $\{\theta = 0\} \cup \{\theta = \pi\}$ in Eqs. (24), are also *standing* (i.e., all phase velocities are zero). Furthermore, from Eq. (24d) it follows that unless $\alpha\beta < 0$ the quantity multiplying $\sin \theta$ is single-signed and all trajectories approach $\mathcal{U}_{\mathcal{R}}$ (see [36,37]), i.e., there are no permanently drifting solutions if $\alpha\beta > 0$. The fact that one can *expect* drifting solutions on the basis of underlying Hamiltonian structure was the conclusion of Section 2.3.

4.1. Principal solutions

We describe here the most important solutions of Eqs. (7), equivalently, Eqs. (24). Many of these solutions (or their analogs) are discussed in [36]. They are summarized, along with the bifurcations they undergo, in Table 2.

- (1) *Standing rolls* ($\text{SR}_1 \in \mathcal{U}_1$). The SR_1 states satisfy $|A_1|^2 = -\lambda/a$, $A_2 = A_3 = 0$. Physically, they represent SW with dominant frequency $m/2$ described by a single wavevector \mathbf{k}_1 . Standing rolls SR_2 with wavevector \mathbf{k}_2 are related to SR_1 through the symmetry κ and are therefore equivalent. Both bifurcate from the flat state (O) when $\lambda = 0$, supercritically if $a < 0$. The eigenvalues of SR_1 within the two-dimensional subspace \mathcal{U}_1 are 0 (a result of the translational symmetry T_{ϕ}) and -2λ . Transverse to \mathcal{U}_1 the eigenvalues ξ have multiplicity two and satisfy

$$a^2 \xi^2 - a(a\mu + \lambda(a - b - d))\xi + \lambda(a - b)(a\mu - d\lambda) + a\beta\lambda = 0. \quad (26)$$

Near onset (i.e., $|\lambda| \ll 1$) these eigenvalues are approximated by μ and $\lambda(a - b + \alpha\beta/\mu)/a$. Thus, the standing rolls SR_1 are stable at onset if $a < 0$ (the bifurcation is supercritical), $\mu < 0$ (stability with respect to perturbations of type A_3 is inherited from the basic flat state), and $\mu(b - a) > \alpha\beta$; they are unstable otherwise.

The SR_1 states undergo a steady-state bifurcation along the line

$$\mu = \frac{\alpha\beta}{b-a} + \frac{d}{a}\lambda, \quad (27)$$

giving rise to a branch of mixed modes (MM) contained in $\mathcal{U}_{\mathcal{R}}$ with $A_2 \neq 0$, $A_3 \neq 0$. They experience a Hopf bifurcation along the line

$$\mu = \frac{b+d-a}{a}\lambda, \quad (28)$$

provided $\alpha\beta < \lambda(a-b)^2/a < 0$. This Hopf bifurcation with $O(2)$ symmetry (see, e.g. [18]) *simultaneously* produces modulated standing waves (MSW) contained in $\mathcal{U}_{\mathcal{R}}$, and DW that break $\mathcal{U}_{\mathcal{R}}$ symmetry. Note that $\alpha\beta < 0$ is a necessary condition for this bifurcation, as it must be if DW are produced. Assuming $\alpha\beta < 0$, the line of Hopf bifurcations (28) intersects the line of steady bifurcations (27) at the Takens–Bogdanov point: $(\lambda, \mu) = \alpha\beta(a, b+d-a)/(b-a)^2$.

- (2) *Standing Rolls* ($SR_3 \in \mathcal{U}_3$). The SR_3 states satisfy $A_1 = A_2 = 0$, $|A_3|^2 = -\mu/e$ and represent harmonic SW (dominant frequency $n/2$) with wavevector \mathbf{k}_3 . They bifurcate from O when $\mu = 0$, supercritically if $e < 0$. Within \mathcal{U}_3 the eigenvalues are 0 and -2μ while the remaining four eigenvalues come in pairs given by

$$s = \lambda - \frac{c}{e}\mu \pm \alpha\sqrt{\frac{-\mu}{e}}. \quad (29)$$

In contrast to SR_1 , only steady-state bifurcations can occur on SR_3 and these generate branches of mixed modes, $MM_{\kappa} \in \mathcal{U}_{\kappa}$ (i.e., the unstable eigenvectors satisfy $|A_1| = |A_2|$).

- (3) *κ -Symmetric mixed modes* ($MM_{\kappa} \in \mathcal{U}_{\mathcal{R}} \cap \mathcal{U}_{\kappa}$). These mixed modes bifurcate, along with SR_1 , from O when $\lambda = 0$. The T_{ϕ} -invariant phase θ must be 0 or π while the amplitudes satisfy

$$(2cd - (a+b)e)r_3^3 \pm (2\alpha d + \beta c)r_3^2 + (2d\lambda + \alpha\beta - (a+b)\mu)r_3 \pm \beta\lambda = 0, \\ r_1^2 = r_2^2 = -\frac{cr_3^2 \pm \alpha r_3 + \lambda}{a+b}, \quad (30)$$

with $\cos \theta$ dictating the \pm sign. Eqs. (30) show that there may be up to three distinct MM_{κ} states for each of the two possible θ values. The additional solutions arise in saddle-node bifurcations, and other transitions can occur as well. Hopf bifurcations lead to modulated standing waves, MSW_{κ} , still contained in $\mathcal{U}_{\kappa} \cap \mathcal{U}_{\mathcal{R}}$, while symmetry-breaking bifurcations lead to drifting waves $DW_{\kappa} \in \mathcal{U}_{\kappa}$ (broken \mathcal{R} symmetry) or to mixed modes $MM \in \mathcal{U}_{\mathcal{R}}$ (broken κ symmetry). The MM states bifurcate from the MM_{κ} branch with $\cos \theta = \text{sign}(\alpha(a-b))$ and do so when

$$\mu = \frac{\alpha\beta}{b-a} + \frac{e}{c}\lambda + \frac{2\alpha(cd-ae)}{c^2(a-b)^2}(a\alpha \pm \sqrt{a^2\alpha^2 - \lambda c(b-a)^2}). \quad (31)$$

- (4) *κ -Symmetric drifting waves* ($DW_{\kappa} \in \mathcal{U}_{\kappa}$). These solutions require $\alpha\beta < 0$. Within Eqs. (7) they drift with constant velocity parallel to $\pm \mathbf{k}_3$ (i.e., $\dot{\theta}_1 = \dot{\theta}_2 = \dot{\theta}_3/2$). Within the four-dimensional reduced system (24) they appear as fixed points with $\theta \neq 0, \pi$ given by

$$r_3^2 = -\frac{\beta(\mu + 2\lambda)}{4\alpha(a+b+d) - \beta(2c+e)}, \quad r_1^2 = r_2^2 = -\frac{2\alpha}{\beta}r_3^2, \\ r_3 \cos \theta = \frac{\mu(2\alpha(a+b) - \beta c) + \lambda(\beta e - 4\alpha d)}{\alpha(4\alpha(a+b+d) - \beta(2c+e))}, \quad (32)$$

and exist in the region

$$(\mu(2\alpha(a+b) - c\beta) - \lambda(4d\alpha - e\beta))^2 \leq (\mu + 2\lambda)\alpha^2(4\alpha\beta(a+b+d) - \beta^2(2c+e)). \quad (33)$$

The DW_κ states can themselves undergo Hopf bifurcations to modulated drifting waves $MDW_\kappa \in \mathcal{U}_\kappa$, as well as symmetry-breaking bifurcations to DW not in \mathcal{U}_κ . This latter bifurcation occurs along the line

$$\mu = \frac{4\alpha(b+d-a) - \beta e}{4\alpha a - \beta c} \lambda. \quad (34)$$

(5) *Mixed modes* ($MM \in \mathcal{U}_\mathcal{R}$). These mixed states (without κ symmetry) satisfy

$$\begin{aligned} r_3^2 &= \frac{\alpha\beta a + (a\mu - d\lambda)(a-b)}{(a-b)(cd - ae)}, & \cos \theta &= \text{sign}(\alpha(a-b)), \\ r_1^2 + r_2^2 &= -\frac{\lambda + cr_3^2}{a}, & r_1 r_2 &= \left| \frac{\alpha}{a-b} \right| r_3. \end{aligned} \quad (35)$$

They form a branch of solutions connecting the SR_1 (SR_2) states with the MM_κ branch having $\cos \theta = \text{sign}(\alpha(a-b))$. There are no saddle-node bifurcations but if $\alpha\beta < 0$ there is an \mathcal{R} symmetry-breaking instability that creates drifting waves DW along the line

$$\mu = \frac{e}{c} \lambda + \frac{\alpha\beta(bc + cd - ac - ae)}{c(a-b)^2}. \quad (36)$$

(6) *Drifting waves* (DW). These steadily drifting solutions (requiring $\alpha\beta < 0$) of Eqs. (7) are not in \mathcal{U}_κ and are therefore free to move in any direction (i.e., their drift direction is determined by the coefficients, not by symmetry). They are represented by fixed points within Eqs. (24) satisfying

$$\begin{aligned} r_3^3 &= \frac{a\mu + (a-b-d)\lambda}{bd + cd - ac - ae}, & r_1^2 + r_2^2 &= -\frac{\lambda + cr_3^2}{a}, \\ \cos^2 \theta &= \frac{(a-b)^2(\lambda + cr_3^2)}{\alpha\beta a}, & r_1 r_2 &= \frac{\alpha r_3 \cos \theta}{a-b}. \end{aligned} \quad (37)$$

As with MM (and DW_κ) there are no saddle-node bifurcations. In fact, for the sets of parameters we investigated there were no additional bifurcations on the DW branch.

(7) *κ -Symmetric modulated standing waves* ($MSW_\kappa \in \mathcal{U}_\mathcal{R} \cap \mathcal{U}_\kappa$). These states appear via Hopf bifurcation from MM_κ . Near the origin $(\mu, \lambda) = (0, 0)$ the bifurcation set is parabolic [38,39]:

$$\mu \simeq -\frac{3e}{|\alpha|} \lambda^2, \quad \alpha\beta e \lambda < 0. \quad (38)$$

The MSW_κ solutions may undergo an \mathcal{R} symmetry-breaking bifurcation to modulated drifting waves MDW_κ and are typically destroyed in a global bifurcation involving a heteroclinic connection between O and SR_3 (see [37,40]).

- (8) *Modulated standing waves* ($MSW \in \mathcal{U}_\mathcal{R}$). These solutions do not have the κ symmetry of MSW_κ . They appear, along with DW, in a Hopf bifurcation on SR_1 .
- (9) *κ -Symmetric modulated drifting waves* ($MDW_\kappa \in \mathcal{U}_\kappa$). These three-frequency states can emerge from DW_κ through a Hopf bifurcation or from MSW_κ via an \mathcal{R} symmetry-breaking bifurcation.
- (10) *Heteroclinic cycles* (HET). There are (at least) three kinds of heteroclinic cycles of relevance to Eqs. (7). Structurally stable heteroclinic cycles (HET_1) connecting two SR_3 solutions, out of phase by π (i.e., related by a translation $T_{(\phi, \pi-\phi)}$), have been well-studied [35,37] in the context of the 1:2 steady-state spatial resonance

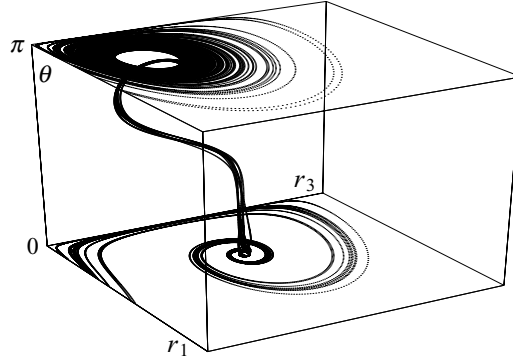


Fig. 6. Chaotic attractor in Eqs. (24) obtained at $(\lambda, \mu) = (-0.0377, 0.035)$ with the coefficients $\alpha = -0.19$, $\beta = 0.166$, $a = -0.0399$, $b = -0.436$, $c = 1.27$, $d = -1.43$, and $e = -0.106$, derived from the Zhang–Viñals model (17) with $m:n = 1:2$, $\Phi = \pi/4$, and (in cgs units) $\omega = 200$, $\nu = 0.01$, $\Gamma = 70$. This attractor is in \mathcal{U}_k and visits the neighborhood of two MM_k fixed points: one with $\theta = 0$ and one with $\theta = \pi$. The latter is near a Hopf bifurcation to MSW_k . The boundary $r_3 = 0$ should be identified at $\theta = 0$ and $\theta = \pi$.

with $\text{O}(2)$ symmetry and in resonant triads as well [36]. They are generic solutions when $\alpha\beta < 0$ that appear at small amplitude ($|\lambda|, |\mu| \ll 1$).

In addition, there are much more intricate heteroclinic cycles (HET_2) involving connections among O , SR_3 , MSW_k , and MM_k (see [40]). Under appropriate conditions, these cycles form near the HET_1 cycles (in a neighboring region of parameter space but further from the origin). The associated dynamics is organized by a sequence of transitions among distinct heteroclinic cycles (one of which is structurally stable) and contains chaos of Shil'nikov type. The type of chaotic attractor one typically finds is shown in Fig. 6.

In the absence of resonance terms (i.e., when $\alpha = \beta = 0$) there are, under certain conditions [36], heteroclinic cycles connecting SR_1 , SR_2 , and SR_3 . The resonance terms in Eqs. (7) destroy these cycles. Nonetheless, for large $m+n$ when resonance effects are diminished, or at values of Φ near $\pm\pi/2$ where the leading order resonance terms vanish (see Eqs. (8)), these “nearby” cycles may yet influence the dynamics.

4.2. Bifurcations: numerical examples

We provide here some numerical examples using coefficients derived from the Zhang–Viñals equations (17). Fig. 7 shows the bifurcations that occur for $m:n = 1:2$, $\Phi = 0$, $\rho = 1$, $\nu = 0.1$, $\Gamma = 21.5$, and $\omega = 200$ (cgs units); for these parameters $\gamma = 0.0341$ and we find $\alpha = -0.265$, $\beta = 0.281$, $a = -6.136$, $b = 0.0266$, $c = -0.98$, $d = -2.076$, and $e = -2.234$. We use $m:n = 1:2$ rather than $m:n = 3:2$ (as in Section 3) mainly for convenience: although the bifurcations seen with other forcing ratios such as $3:2$ (and comparable physical parameters) are the same as those found in Fig. 7 they tend to be somewhat more bunched together thus more difficult to illuminate. The use of $1:2$ forcing also has the advantage of the large $\mathcal{O}(1/\gamma)$ oscillations with Φ in b , c , and d (see Eqs. (8)); this leads to greater control over the normal form coefficients and hence to a wider range of dynamical possibilities (for example, this Φ dependence made it easier to find the interesting heteroclinic behavior shown in Fig. 6).

If one traverses the clockwise circular path shown in Fig. 7 the resulting bifurcation diagram is that of Fig. 8. Initially, in the third quadrant of the (λ, μ) plane, all initial conditions are attracted to the stable flat state O . As the polar angle (ϕ , say) is decreased through π this flat state becomes unstable to (a circle of) standing rolls of type SR_3 . At $\phi \simeq 2.64$ (point 1 in Fig. 8) these stable SR_3 states undergo a supercritical symmetry-breaking bifurcation to (a torus of) κ -symmetric mixed modes MM_k satisfying $\theta = \pi$. These MM_k states are stable until a subcritical

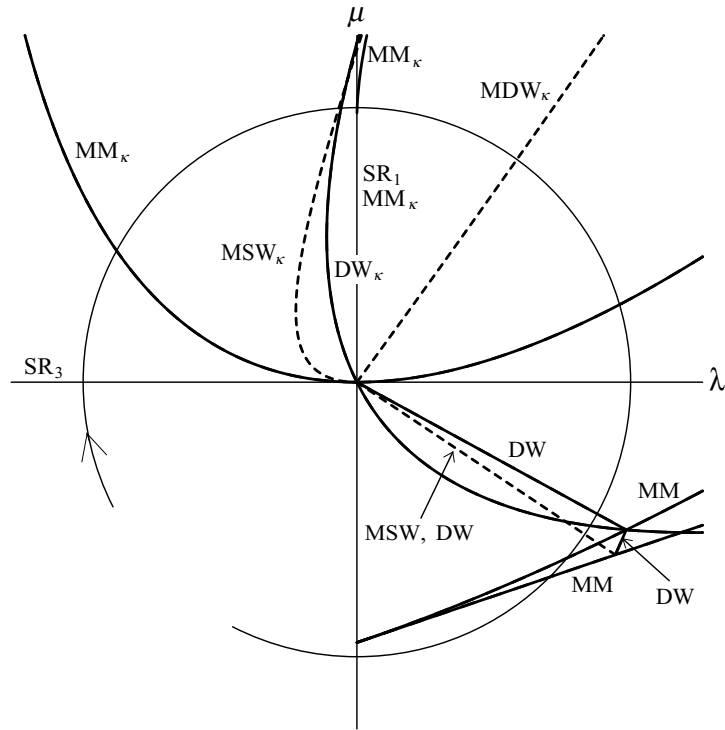


Fig. 7. Bifurcation sets for the case $m:n = 1:2$ and $\Phi = 0$ with (in cgs units) $\rho = 1$, $\nu = 0.1$, $\Gamma = 21.5$, and $\omega = 200$. Curves are labeled by the solutions created (see text) and are dashed in the case of Hopf bifurcation. The clockwise circular path is used to generate the bifurcation diagram in Fig. 8 and is at a radius $\sqrt{\lambda^2 + \mu^2} = 0.0128$.

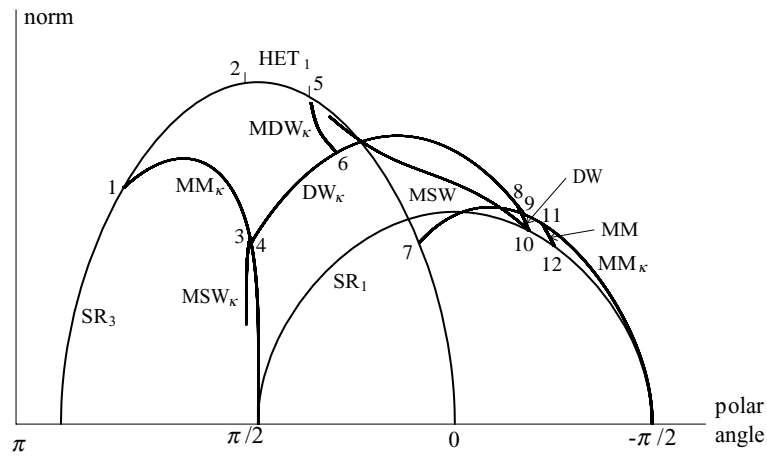


Fig. 8. Bifurcation diagram for the clockwise circular path shown in Fig. 7.

Hopf bifurcation at $\phi \simeq 1.64$ (point 3) producing κ -symmetric modulated standing waves MSW_κ . The MSW_κ are themselves destroyed in a heteroclinic bifurcation (point 2, marked by a small dash on the SR_3 branch) joining O and SR_3 (see [40]) at $\phi \simeq 1.67$. The same global bifurcation marks the birth of structurally (and asymptotically) stable heteroclinic cycles (HET_1) connecting points on the circle of SR_3 states to their “ π translates”. After the Hopf bifurcation renders MM_κ unstable the heteroclinic cycles HET_1 are the only attractors of the system (7). These HET_1 remain stable until $\phi \simeq 1.16$ (point 5; this is when $\mu = \lambda e/c$ and the two eigenvalues of Eq. (29), one positive and one negative, are of equal magnitude). The bifurcation that occurs here simultaneously produces stable MDW_κ and unstable MSW (the fact that the MSW branch does not visibly originate here is due to numerical limitations). The stable MTW_κ branch describes modulations of ever decreasing amplitude as it approaches the branch of DW_κ states, themselves present since an \mathcal{R} symmetry-breaking bifurcation on MM_κ at $\phi \simeq 1.63$ (point 4), and is destroyed in a Hopf bifurcation at $\phi \simeq 0.95$ (point 6). The DW_κ are then stable until a supercritical κ symmetry-breaking bifurcation to DW at $\phi \simeq -0.5$ (point 8); this occurs just prior to their termination at $\phi \simeq -0.55$ (point 9) on the *other* MM_κ branch, i.e., the one with $\theta = 0$ existing between $\phi = -\pi/2$ and a bifurcation from SR_3 at $\phi \simeq 0.29$ (point 7). The stable DW branch terminates, along with the unstable MSW branch, in a Hopf bifurcation on SR_1 at $\phi \simeq -0.59$ (point 10). The SR_1 rolls are stable between this Hopf bifurcation and a subcritical bifurcation to MM at $\phi \simeq -0.79$ (point 12). This MM branch also connects to (and stabilizes) the MM_κ branch at $\phi \simeq -0.7$ (point 11). Finally, the MM_κ states (with $\theta = 0$) are stable between this last bifurcation and $\phi = -\pi/2$ where they vanish, along with SR_1 , restoring stability to the flat state.

If, in contrast to the case of Fig. 7, one adjusts the forcing phases so that $\Phi = \pi/2$ then the (leading order) expressions for α and β of Eqs. (8) vanish. With the same physical parameters as Fig. 7 it turns out that the first nonvanishing contributions have the *same* algebraic sign, i.e., $\alpha\beta > 0$. Specifically, we find $\alpha = 0.0784$,

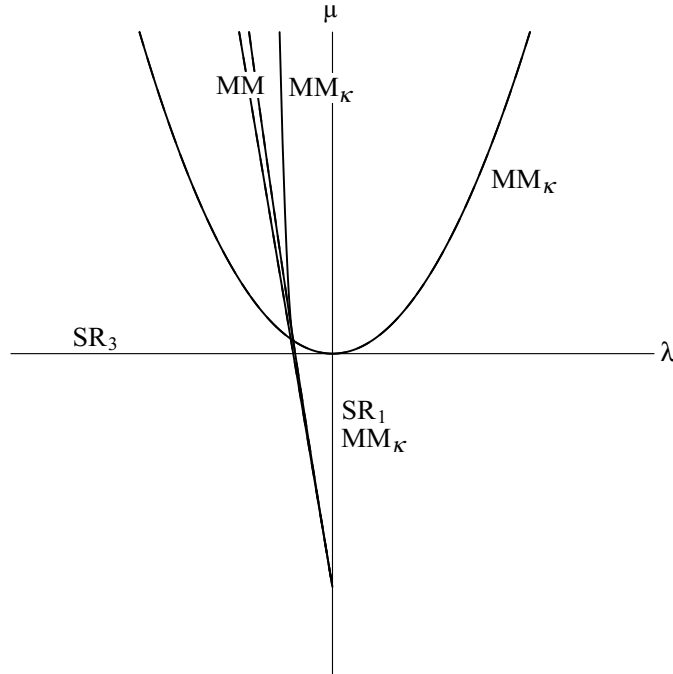


Fig. 9. Bifurcation sets for $m:n = 1:2$ with the same parameters as Fig. 7 except that $\Phi = \pi/2$. For this choice of phase $\alpha\beta > 0$ and there are no DW_κ , MDW_κ , DW , MSW_κ , MSW , or heteroclinic solutions.

$\beta = 0.0744$, $a = 0.549$, $b = -0.523$, $c = -0.0155$, $d = -3.266$, and $e = -2.227$. The fact that $\alpha\beta > 0$ explains the dramatically different (and less rich) unfolding shown in Fig. 9. In this case there are no drifting solutions (DW_κ , MDW_κ , DW) or heteroclinic cycles (HET_1 , HET_2). Furthermore, there are no modulated standing waves MSW_κ or MSW (it was shown in [38] that $\alpha\beta < 0$ is necessary for MSW_κ). A second, somewhat surprising, feature of the $\Phi = \pi/2$ coefficients is the large change in the self-interaction coefficient a : it is now positive whereas at $\Phi = 0$ it was -6.136 . Such substantial Φ dependence is not an ingredient of Eqs. (8) and is a result of “1:2” linear resonances, i.e., harmonic modes satisfying $k = 2k_1$ or $k = 2k_2$. The influence of these damped modes (see [10]) is especially strong here because $k_3 \approx 1.86$ is quite close to $2k_1 \approx 1.94$ (the damping of the $2k_1$ modes is thus very small and they nearly satisfy the 1:2 temporal resonance condition $m = \Omega(2k_1)$; in this case $m = n/2$). For comparison, note that the $2k_3$ modes experience much stronger damping and the relevant self-interaction coefficient e shows no significant dependence on Φ , in agreement with Eqs. (8). Because $a > 0$ the bifurcation of SR_1 and MM_κ from the flat state is now subcritical (observe how the MM bifurcations from SR_1 and MM_κ have switched to the left side of $\lambda = 0$ in Fig. 9) and the cubic truncation (7) is no longer well-behaved (some trajectories diverge).

5. Conclusions

The weakly nonlinear dynamics of a class of resonant triads occurring in the vicinity of the bicritical point of the two-frequency forced Faraday problem has been studied in detail. The approach taken for this resonant triad can be easily extended to a wide range of patterns produced by multi-frequency forcing (see [9]), and is based on very general symmetry considerations. In particular, we make use of the fact that the weakly damped problem possesses additional structure beyond the more obvious spatial and discrete temporal symmetries, i.e., it must satisfy the constraints of continuous time translation and time reversal (viewed as parameter symmetries) and respect the nearby Hamiltonian structure of the undamped problem. The effect of these “broken” symmetries is straightforward to establish in the context of TW equations (5), and in the reduced SW equations (7) reveals itself in the structure of the normal form coefficients (8). Most notably, we found that the coefficients α and β in Eqs. (7) could be expected to be of opposite sign, exhibit simple harmonic dependence on the phase Φ , and scale as the damping γ to the power $(m + n - 3)/2$. Each of these predictions was supported in the direct numerical calculation of coefficients from the Zhang–Viñals equations (17). Moreover, the exponential decrease in the size of the resonance terms with $m + n$ provides an explanation for the lack of experimental observations [3,8] of this triad with large values of m and n . Recall, however, that this simple prediction (and the other scaling laws) emerged after we expanded the SW normal form coefficients in powers of f_m , f_n , and γ (see Eqs. (6)). Particularly in the case of γ it is not clear that the assumption of analyticity is a good one—the addition of damping is known to act as a singular perturbation (see, e.g. [41,42]). For the quasipotential equations of Zhang and Viñals the numerical agreement (and hence the justification for a simple Taylor expansion) is quite convincing, but we speculate that a more rigorous treatment using the Navier–Stokes equations with realistic boundary conditions and finite fluid depth may lead to a departure, in some regimes, from the scalings given here. This departure will presumably be small in weakly damped systems of large depth where the Zhang–Viñals equations are expected to apply.

The resonant triad system (7) exhibits extremely rich dynamics, much more so in the case where the resonant coefficients satisfy $\alpha\beta < 0$. That the underlying Hamiltonian structure makes this the typical case for weak damping and, furthermore, that this situation depends on the relative phase of the two forcing terms, is a result we have emphasized throughout this paper. When $\alpha\beta < 0$ there exist several types of modulated standing waves, drifting waves (of both steady and modulated character), and heteroclinic cycles with associated phenomena like the chaotic attractor of Fig. 6. It must be admitted, however, that none of these more complicated solutions have yet been seen in experiment; other than simple roll states, only the mixed mode MM_κ has been established experimentally [8]. It

is quite possible that the remaining solutions are simply unstable when all types of perturbations are considered (the system may prefer hexagons or squares, for instance). It might also be that the use of finite containers plays a critical role in preventing many of these solutions from appearing (the drifting waves DW_κ , DW , and MTW_κ obviously cannot exist as such in nonperiodic bounded domains). It would be interesting to see if a more deliberate search, perhaps in a very large aspect ratio container, would reveal more features of the dynamics presented in Section 4. On the other hand, it would miss the point to focus too narrowly on the resonant triad treated here. This paper is also intended to serve as a detailed illustration of a very general method with wide applicability to parametrically forced problems, particularly those with forcing functions composed of multiple frequencies – for example, in [9] we considered two-frequency forced hexagons and two-mode superlattices [5]. The symmetry-based approach of this paper provides, for weakly damped systems, a means of determining scaling laws and other important qualitative features of the normal form coefficients without resorting to a full center manifold reduction from the governing equations (often an exceedingly difficult task). The results also suggest how one might begin to think about designing forcing functions that enhance, suppress, or otherwise control the patterns of interest (for example, superlattices). This very intriguing direction will be pursued elsewhere [43].

Acknowledgements

We thank J. Fineberg, M. Golubitsky, E. Knobloch, H. Riecke, P. Umbanhowar, and in particular, C.M. Topaz for very helpful discussions. This work was supported by NASA Grant No. NAG3-2364, NSF Grant No. DMS-9972059, and by the NSF MRSEC Program under DMR-0213745.

Appendix A

We give here the expressions for J_1, \dots, J_7 appearing in Eqs. (8):

$$J_1 = \frac{2Q_r^2}{\tilde{\mu}_i^2} \left(\hat{v}_n + \frac{v_r \tilde{\lambda}_n}{\tilde{\lambda}_i} - v_n C_1 \right), \quad \text{where } C_1 = \frac{v_\gamma}{v_r} + \frac{v_m v_r}{\tilde{\lambda}_i^2} + \frac{v_n Q_r^2}{v_r \tilde{\mu}_i^2}, \quad (\text{A.1})$$

$$J_2 = \frac{2v_r^2}{\tilde{\lambda}_i^2} \left(\hat{Q}_m + \frac{Q_r \tilde{\mu}_m}{\tilde{\mu}_i} - Q_n C_2 \right), \quad \text{where } C_2 = \frac{Q_\gamma}{Q_r} + \frac{Q_m v_r^2}{Q_r \tilde{\lambda}_i^2} + \frac{Q_n Q_r}{\tilde{\mu}_i^2}, \quad (\text{A.2})$$

$$J_3 = a_r + b_r - C_1(a_i + b_i) + \frac{v_r}{\tilde{\lambda}_i}((r_2)_i - (q_1)_i - (q_2)_i), \quad (\text{A.3})$$

$$J_4 = l_r + p_r - C_2(l_i + p_i) + \frac{Q_r}{\tilde{\mu}_i}((u_3)_i - (s_3)_i - (s_4)_i), \quad (\text{A.4})$$

$$J_5 = \delta_r + c_r + d_r - C_1(\delta_i + c_i + d_i) + \frac{v_r}{\tilde{\lambda}_i}((r_3)_i - (r_1)_i - (q_3)_i - (q_4)_i), \quad (\text{A.5})$$

$$J_6 = e_r + f_r - C_1(e_i + f_i) - \frac{v_r}{\tilde{\lambda}_i}((q_5)_i + (q_6)_i) + \frac{Q_r}{\tilde{\mu}_i}((r_5)_i - (r_4)_i), \quad (\text{A.6})$$

$$J_7 = g_r + h_r - C_2(g_i + h_i) - \frac{Q_r}{\tilde{\mu}_i}((s_1)_i + (s_2)_i) + \frac{v_r}{\tilde{\lambda}_i}((u_2)_i - (u_1)_i). \quad (\text{A.7})$$

References

- [1] M. Faraday, On the forms and states of fluids on vibrating elastic surfaces, *Phil. Trans. Roy. Soc. Lond.* 121 (1831) 319–340.
- [2] D. Binks, W. van de Water, Nonlinear pattern formation of Faraday waves, *Phys. Rev. Lett.* 78 (1997) 4043–4046.
- [3] H. Arbell, J. Fineberg, Pattern formation in two-frequency forced parametric waves, *Phys. Rev. E* 65 (2002) 036224.
- [4] W.S. Edwards, S. Fauve, Patterns and quasi-patterns in the Faraday experiment, *J. Fluid Mech.* 278 (1994) 123–148.
- [5] H. Arbell, J. Fineberg, Spatial and temporal dynamics of two interacting modes in parametrically driven surface waves, *Phys. Rev. Lett.* 81 (1998) 4384–4387.
- [6] A. Kudrolli, B. Pier, J.P. Gollub, Superlattice patterns in surface waves, *Physica D* 123 (1998) 99–111.
- [7] T.B. Benjamin, F. Ursell, The stability of a plane free surface of a liquid in vertical periodic motion, *Proc. Roy. Soc. Lond. A* 225 (1954) 505–515.
- [8] H. Arbell, J. Fineberg, Two-mode rhomboidal states in driven surface waves, *Phys. Rev. Lett.* 84 (2000) 654–657.
- [9] J. Porter, M. Silber, Broken symmetries and pattern formation in two-frequency forced Faraday waves, *Phys. Rev. Lett.* 89 (2002) 084501.
- [10] C.M. Topaz, M. Silber, Resonances and superlattice pattern stabilization in two-frequency forced Faraday waves, *Physica D* 172 (2002) 1–29.
- [11] M. Silber, A.C. Skeldon, Parametrically excited surface waves: two-frequency forcing, normal form symmetries and pattern formation, *Phys. Rev. E* 59 (1999) 5446–5456.
- [12] H.W. Müller, Periodic triangular patterns in the Faraday experiment, *Phys. Rev. Lett.* 71 (1993) 3287–3290.
- [13] C. Wagner, H.W. Müller, K. Knorr, Crossover from a square to a hexagonal pattern in Faraday surface waves, *Phys. Rev. E* 62 (2000) R33–R36.
- [14] W. Zhang, J. Viñals, Pattern formation in weakly damped parametric surface waves, *J. Fluid Mech.* 336 (1997) 301–330.
- [15] W. Zhang, J. Viñals, Pattern formation in weakly damped parametric surface waves driven by two frequency components, *J. Fluid Mech.* 341 (1997) 225–244.
- [16] M. Silber, C.M. Topaz, A.C. Skeldon, Two-frequency forced Faraday waves: weakly damped modes and pattern selection, *Physica D* 143 (2000) 205–225.
- [17] S.T. Milner, Square patterns and secondary instabilities in driven capillary waves, *J. Fluid Mech.* 225 (1991) 81–100.
- [18] M. Golubitsky, I. Stewart, D.G. Shaeffer, *Singularities and Groups in Bifurcation Theory*, vol. 2, Springer-Verlag, New York, 1988.
- [19] J.D. Crawford, E. Knobloch, Symmetry and symmetry-breaking bifurcations in fluid mechanics, *Annu. Rev. Fluid Mech.* 23 (1991) 341–387.
- [20] H. Riecke, J.D. Crawford, E. Knobloch, Time-modulated oscillatory convection, *Phys. Rev. Lett.* 61 (1988) 1942–1945.
- [21] H. Riecke, M. Silber, L. Kramer, Temporal forcing of small-amplitude waves in anisotropic systems, *Phys. Rev. E* 49 (1994) 4100–4113.
- [22] J.W. Swift, Hopf bifurcation with the symmetry of the square, *Nonlinearity* 1 (1988) 333–377.
- [23] W. Zhang, Pattern formation in weakly damped parametric surface waves, Ph.D. Thesis, Florida State University, 1994.
- [24] J.D. Crawford, Introduction to bifurcation-theory, *Rev. Mod. Phys.* 63 (1991) 991–1037.
- [25] K. Kumar, L.S. Tuckerman, Parametric instability of the interface between two fluids, *J. Fluid Mech.* 279 (1994) 49–68.
- [26] V.E. Zakharov, Stability of periodic waves of finite amplitude on the surface of deep fluid, *J. Appl. Mech. Tech. Phys.* 2 (1968) 190–194.
- [27] J.W. Miles, On Hamilton's principle for surface waves, *J. Fluid Mech.* 83 (1977) 153–158.
- [28] L.J.F. Broer, On the Hamiltonian theory of surface waves, *Appl. Sci. Res.* 29 (1974) 430–446.
- [29] P. Lyngshansen, P. Alstrom, Perturbation theory of parametrically driven capillary waves at low viscosity, *J. Fluid Mech.* 351 (1997) 301–344.
- [30] A.C. Radder, An explicit Hamiltonian formulation of surface waves in water of finite depth, *J. Fluid Mech.* 237 (1992) 435–455.
- [31] J.W. Miles, Nonlinear Faraday resonance, *J. Fluid Mech.* 146 (1984) 285–302.
- [32] V.P. Krasitskii, On reduced equations in the Hamiltonian theory of weakly nonlinear surface waves, *J. Fluid Mech.* 272 (1994) 1–20.
- [33] P. Chossat, F. Dias, The 1:2 resonance with $O(2)$ symmetry and its applications in hydrodynamics, *J. Nonlinear Sci.* 5 (1995) 105–129.
- [34] P. Chossat, The bifurcation of heteroclinic cycles in systems of hydrodynamical type, *Dynam. Cont. Dis. Ser. A* 8 (2001) 575–590.
- [35] C.A. Jones, M.R.E. Proctor, Strong spatial resonance and traveling waves in Benard convection, *Phys. Lett. A* 121 (1987) 224–228.
- [36] J. Guckenheimer, A. Mahalov, Resonant triad interactions in symmetric systems, *Physica D* 54 (1992) 267–310.
- [37] D. Armbruster, J. Guckenheimer, P. Holmes, Heteroclinic cycles and modulated traveling waves in systems with $O(2)$ symmetry, *Physica D* 29 (1988) 257–282.
- [38] G. Dangelmayr, Steady-state mode interactions in the presence of $O(2)$ -symmetry, *Dynam. Stabil. Syst.* 1 (1986) 159–185.
- [39] M.R.E. Proctor, C.A. Jones, The interaction of two spatially resonant patterns in thermal convection. Part 1. Exact 1:2 resonance, *J. Fluid Mech.* 188 (1988) 301–335.
- [40] J. Porter, E. Knobloch, New type of complex dynamics in the 1:2 spatial resonance, *Physica D* 159 (2001) 125–154.
- [41] O.M. Phillips, *The Dynamics of the Upper Ocean*, Cambridge University Press, Cambridge, 1977.
- [42] C. Martel, E. Knobloch, Damping of nearly inviscid water waves, *Phys. Rev. E* 56 (1997) 5544–5548.
- [43] J. Porter, C.M. Topaz, M. Silber, Pattern selection via multi-frequency parametric forcing, Preprint.